Proceedings of the Korean Superconductivity Society Meeting 2000
(KSS 2000), YongPyung, Kangwondo, Korea, Aug. 16-18, 2000

Effects of post-annealing temperature of CeO_2 buffer layers on the surface morphology, structures and microwave properties of $YBa_2Cu_3O_{7-\delta}$ films on sapphire

W. I. Yang, J. H. Lee, J. S. Ryu, Y. B. Ko, Y. S. Chung,
Jung Hur[+] and Sang Young Lee
Department of Physics and Center for Advanced Materials and Devices
[+]*Department of Electronic Engineering*
Konkuk University
Seoul 143-701, Korea

Abstract

Effects of the post-annealing temperature of CeO_2 buffer layers on the properties of YBCO films on CeO_2-buffered sapphire were investigated. 45 nm-thick CeO_2 buffer layer was prepared in-situ on r-cut sapphire using an on-axis rf magnetron sputtering method, which was later post-annealed at temperatures between 950 °C and 1100 °C in an oxygen-flowing environment. YBCO films were prepared on CeO_2-buffered sapphire (CbS), for which the surface morphology, crystal structures and electrical properties of the YBCO films were studied. YBCO films on post-annealed CbS appeared to have better properties than those on as-grown CbS with regard to the morphological, structural and electrical properties when the YBCO films were prepared on CeO_2 buffer layer post-annealed at temperatures of 1000 – 1050 °C. A TE_{011} mode rutile-loaded cylindrical cavity resonators was fabricated with the YBCO films placed as the endplates, for which the unloaded Q of the resonator was measured. It turned out that the resonator with the endplates prepared from the YBCO films on post-annealed CbS at 1000 °C showed the highest unloaded Q with the value more than 8×10^5 at 30 K and 8.6 GHz, revealing that the YBCO films on post-annealed CbS at 1000 °C the temperature could be the lowest among the YBCO films on post-annealed CbS.

I. Introduction

To date, sapphire substrates are widely used in preparing YBCO films for high power microwave applications. Advantages in using sapphire include that i) the thermal conductivity of sapphire is less than 1/20 compared to LAO, ii) its loss tangent ($\tan\delta$) is extremely low with the respective value of about 5×10^{-6} and 10^{-7} at 300 K and 77 K [2], and iii) large sapphire substrates with the diameter more than 4 inches are available. Despite the chemical stability of sapphire in high temperature environments, direct deposition of YBCO on sapphire is limited by chemical interaction between sapphire and YBCO. To prevent such interaction, CeO_2 films have been used as the buffer layers on r-cut sapphire because of the chemical inertness of CeO_2 against both YBCO (up to 790 °C) [3] and Al_2O_3 (up to 1000 °C) [4]. Also, the structure of sapphire along the (1102) plane, (or r-plane) is nearly rectangular with the atomic spacing along the quasi-orthogonal directions of [1011] and [1210] in the r-plane being 0.512 nm and 0.4759 nm, respectively. The values correspond to the respective lattice mismatch of 5.7 % and 13.7 % sapphire and cubic CeO_2 structure (lattice parameter a = 0.5411nm). Furthermore, the lattice mismatch between CeO_2 and YBCO is less than 1 %, enabling epitaxial growth of YBCO on a CeO_2 layer. Besides, strains caused by different thermal expansion coefficients of the YBCO film ($\alpha_{YBCO}=13 \times 10^{-6}$ K^{-1})

and the substrate (α_{Al2O3} = 6 x 10^{-6} K^{-1}) can be reduced by using a CeO_2 buffer layer since α_{CeO2} = 11.6 X $10^{-6}K^{-1}$, the value between α_{YBCO} and α_{Al2O3}.

The surface resistance ($R_{S,YBCO}$) of YBCO films on CbS have been reported low enough to meet the requirements for microwave devices in transmitter modules [1]. Considering that YBCO on CbS is applicable for making Josephson junctions for SQUIDs, YBCO films with smaller surface roughness would be more useful in preparing Josephson junctions with improved parameters. Furthermore, as far as digital application of YBCO at the frequency of several GHz is concerned, both small surface roughness and low $R_{S,YBCO}$ are important to realize digital devices of high performance. We previously reported that both $R_{S,YBCO}$ and the surface morphology of YBCO films on CbS can be greatly improved by using post-annealed CbS at 1000 C, with the typical peak-to-valley surface roughness of about 3 nm and $R_{S,YBCO}$ of about ~ 300 μΩ at 77 K and 10 GHz for 300 nm-thick YBCO films. However, Attempts have been made to improve the surface roughness of the CeO_2 buffer layer either by using post-annealed sapphire substrate [5] or by post-annealing the CeO_2 buffer layer [6]. However, up to our knowledge, no report has yet been made on successful fabrication of YBCO films on CbS with the surface roughness of less than several nanometers when the film thickness is more than 300 nm.

Various deposition methods have been used in growth of epitaxial CeO_2 films on r-cut sapphire substrates, which include electron-beam evaporation [7, 8], laser ablation [9, 10], metalorganic chemical vapor deposition (MOCVD) [11, 12], and magnetron sputtering [1,2,13]. It is known that the surface morphology of the CeO_2 film, its crystallinity, orientation and the oxygen stoichiometry are strongly dependent on the deposition conditions. However, the relations between the deposition conditions and the properties of CeO_2 films are not clearly understood.

In this paper, structures and electrical properties of YBCO films grown on post-annealed CbSs at various temperatures are described. Effects of post-annealing of CeO_2 buffer layers on the structures and the electrical properties of YBCO films were studied here. Microwave surface resistance of 400 nm-thick YBCO films on post-annealed CbS were measured. Optimum conditions for realizing YBCO films with better surface morphology and microwave properties were discussed.

II. Experimental

45 nm-thick CeO_2 buffer layers were grown in-situ on 12 x 12 x 0.5 mm^3 r-cut sapphire using an on-axis RF magnetron sputtering method. During deposition of CeO_2, the deposition rate was 0.75 nm/sec with the total pressure of 70 mtorr, Ar/O_2 ratio of 3:1 and the substrate temperature (T_S) of 780 °C. We also prepared the post-annealed CeO_2 buffer layers by heat treatment of the as-grown CeO_2 buffer layers at 950 - 1100 °C for an hour inside a furnace. Later 400 nm-thick YBCO films were deposited on r-cut sapphire with a 45 nm-thick CeO_2 buffer layer by an off-axis *dc* magnetron sputtering method at the rate of 1.1 nm/sec. For deposition of YBCO, we used T_S = 730 °C, the dc power of 60 W with the total gas pressure of 100 mtorr and Ar/O_2 ratio of 3:1. X-ray diffraction (XRD), atomic force microscope (AFM), and SEM were used for investigating the structures of the CeO_2 buffer layers and the YBCO films. The conventional four-probe method was used for measuring the dc resistance of the YBCO films. TE_{011} mode unloaded Qs (Q_0) of a rutile-loaded cavity resonator were measured using the YBCO films as the endplates, where a rutile rod was sandwiched between two YBCO endplates of a cylindrical cavity made of oxygen-free high purity copper (OFHC). The rutile rod, supplied by Crystec, has the dimensions of 3.88 mm and 2.73 mm for the diameter and height, respectively, with the corresponding values of 9 mm and 2.73 mm for the dimensions of the cylindrical cavity. A HP8510C network analyzer was used in measuring the TE_{011} mode Q_0. More details for measurement procedures have been reported elsewhere [14].

III. Results and Discussion

III. 1. Surface Morphology and Structures of CeO_2 layers

AFM data for the 45 nm-thick CeO_2 layers revealed that the peak-to-valley distance in the surface profile (henceforth called 'the *R*-factor') decreased somewhat

Table 1. The surface roughness and structural properties of as-grown and post-annealed CeO_2-buffered sapphire (CbS) prepared under different conditions.

Sample No.	Smoothness (Å)	2θ-FWHM	Rocking curve FWHM	Lattice Constance
Ce-A	Peak to valley 38 Rms 9.2	(200) 0.248 (400) 0.314	(200) 0.382 (400) 0.52	(200) 5.4078
Ce-P1	Peak to valley 9.2 Rms 2.72	(200) 0.23 (400) 0.392	(200) 0.457 (400) 0.50	(200) 5.4110
Ce-P2	Peak to valley 15 Rms 3.1	(200) 0.25 (400) 0.4	(200) 0.49 (400) 0.5	(200) 5.4110
Ce-P3	Peak to valley 6.9 Rms 2.1	(200) 0.23 (400) 0.38	(200) 0.42 (400) 0.45	(200) 5.4046
Ce-P4	Peak to valley 1.4 Rms 3.7	(200) 0.213 (400) 0.353	(200) 0.36 (400) 0.38	(200) 5.4014

when the as-grown CeO_2 layers were post-annealed at temperature higher than 950 °C. For instance, the *R*-factor of the as-grown sample Ce-A was 3.8 nm, which became as small as 0.92 nm (Ce-P1), 1.5 nm (Ce-P2), 0.69 nm (Ce-P3) and 1.4 nm (Ce-P4) after post-annealing of sample Ce-A at the temperature of 950 °C, 1000 °C, 1050 °C and 1100 °C, respectively. Figs. 1(a) and 1(b) show the AFM images for samples Ce-A and Ce-P2. It is noted that our results are consistent with previously reported ones [6, 15], where improvements in the R-factor have been observed.

XRD data of both as-grown and post-annealed CeO_2 buffer layers showed only (*l*00) peaks,

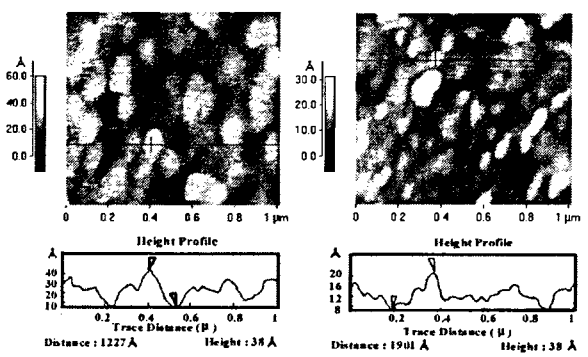

Fig. 1. AFM pictures of a 45 nm-thick CeO_2 film on a r-cut sapphire (a) before annealing (sample Ce-A) and (b) after annealing at 1000 °C (sample Ce-P2).

indicating epitaxial growth of CeO_2 layers on r-cut sapphire. The full width at half maximum (FWHM) of $\Delta(\theta\text{-}2\theta)$ reflex and the FWHM ($\Delta\omega$) from the rocking curve data for the (400) peak appeared to be 0.31 ° and 0.52° for sample Ce-A. $\Delta\omega$s of post-annealed CeO_2 appeared smaller than that of as-grown CeO_2 with the values of 0.50 °, 0.50 °, 0.45 ° and 0.38° for sample Ce-P1 ~ Ce-P4, revealing improved crystalline structures of CeO_2 after the post-annealing. The calculated lattice constants were 0.541 nm for samples Ce-P1 and Ce-P2, with a smaller value of 0.540 nm for samples Ce-P3 and Ce-P4. Detailed results for CeO_2 layers are listed in Table 1. The improved surface roughness in the post-annealed CeO_2 films such as Ce-P1 ~ Ce-P4 seems due to the surface diffusion of Ce atoms caused by the post-annealing process at temperatures higher than 950 °C.

III. 2. Surface Morphology, Structures and Microwave Properties of YBCO Films

We also prepared 400 nm-thick YBCO films on as-grown CbS (samples YBCO-A) and on post-annealed CbSs (samples YBCO-P1 ~ YBCO-P4). For this purpose, we used Ce-A and Ce-P1 ~ Ce-P4. XRD data revealed that all the YBCO films were epitaxially grown along the c-axis regardless of the post-annealing treatment for the CeO_2 buffer layers. Fig. 2(a) shows the XRD data for a YBCO film on a post-annealed CbS at 1000 °C (sample YBCO-P2), where only (00*l*) peaks are seen with the FWHM of (θ - 2θ) reflex of (005) peak being 0.19°. $\Delta\omega$ for the (005) peak of the YBCO film appeared to be 0.48° for sample YBCO-P2 as seen in Fig. 2(b), with the value much smaller than $\Delta\omega$ = 0.65 ° for the YBCO film on as-grown CeO_2 (sample YBCO-A). $\Delta\omega$ for the (005) peak of YBCO films on post-annealed CbS at 1050 °C and 1100 °C (samples YBCO-P3 and YBCO-P4) appeared much smaller than that of YBCO-A with the respective value of 0.46 ° and 0.47 °, revealing significant improvements in the crystalline quality of YBCO films on post-annealed CbS. Furthermore, the resistance data of YBCO films on post-annealed CbS appeared better than the

Table 2. Data for 300 nm-thick YBCO films on r-cut sapphire substrates buffered with as-grown and post-annealed 45 nm-thick CeO_2 layers. The post-annealing temperature for the CeO_2 buffer layer is from 950 °C to 1100 °C.

Sample No.	Smoothness (Å)	2θ-FWHM	Rocking curve FWHM
YBCO-A	Many hillocks 963 *Rms* : 284	(200) 0.25 (400) 0.5 (005) 0.2	(200) 0.5 (400) 0.57 (005) 0.65
YBCO-P2	45 rms : 11	(200) 0.25 (400) 0.42 (005) 0.19	(200) 0.5 (400) 0.5 (005) 0.48
YBCO-P3	79 rms : 31	(200) 0.23 (400) 0.42 (005) 0.19	(200) 0.52 (400) 0.49 (005) 0.46
YBCO-P4	86 rms : 19	(200) 0.24 (400) 0.38 (005) 0.16	(200) 0.4 (400) 0.42 (005) 0.47

ones of YBCOs on as-grown CbS. For instance, the transition width (ΔT) and *R(300K)/R(100K)* ratio are 1 K and 3, respectively, for YBCO-P2 ~ YBCO-P4, while the corresponding values are 2 K and 2.8, respectively, for YBCO-A. Above all, the surface smoothness of YBCOs on post-annealed CbS appeared dramatically improved compared to that of YBCOs on as-grown CbS. AFM pictures revealed that the *R*-factor was 96 nm for sample YBCO-A, while the values became significantly smaller with the magnitudes of 4.5 nm, 7.9 nm and 8.6 nm for samples YBCO-P2 ~ YBCO-P4, respectively. Figs. 3(a) and 3(b) show AFM images of samples YBCO-A and YBCO-P2. Detailed results for the YBCO films are listed in Table 2. As seen in Fig. 3(a), the observed high R-factors for YBCOs on as-grown CbS are mainly attributed to outgrowths of YBCO. Meanwhile, outgrowths were rarely observed for YBCO films on post-annealed CbSs as seen in Fig. 3(b) for sample YBCO-P2, allowing very small R-factors. It is noted that no microcracks were observed in the SEM images of all the YBCO samples.

Our results are consistent with our previous reports on 140 nm-thick and 300 nm-thick YBCO films on post-annealed CbSs, where the R-factor appeared to be as small as 3.2 nm for the 300 nm-thick YBCO film on post-annealed CbS at 1000 °C [16]. We note here that the R-factor of the YBCO film on CbS became the smallest when the CbS was post-annealed at 1000 °C, with those of the YBCO films on CbSs post-annealed at higher temperatures of 1050 °C and 1100 °C appearing higher. The correct reasons for significant improvement in the surface smoothness of the YBCO films on post-annealed CbS are yet to be investigated. Our observation is also similar to what has previously been reported for YBCO films on post annealed MgO [17], where the improved surface roughness was attributed to the formation of atomic steps on the surface of the post-annealed CeO_2 buffer layers, with

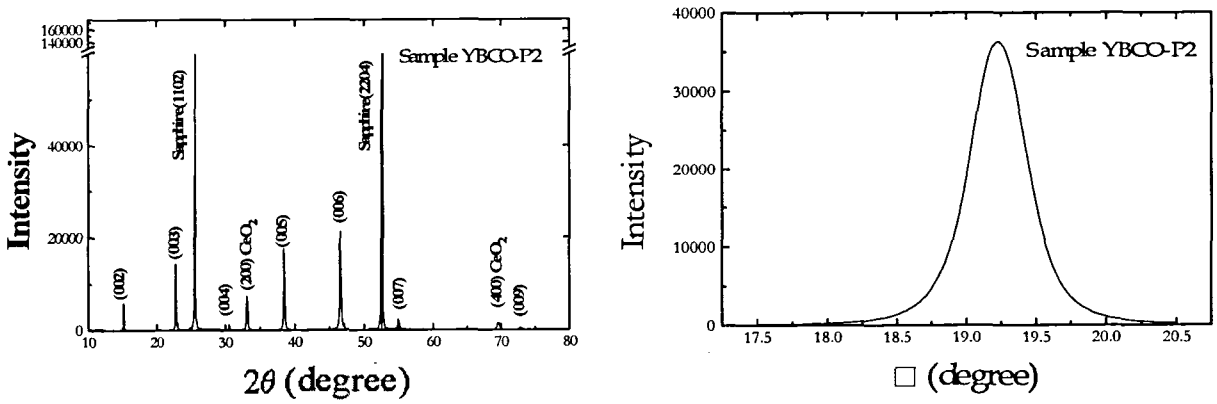

Fig. 2. (a) X-ray diffraction data of a 400 nm-thick YBCO film (sample YBCO-P2) on r-cut sapphire buffered with a 45 nm-thick CeO_2 layer post-annealed at 1000 °C. (b) ω-scan of the (005) peak of sample YBCO-P2. The FWHM value is 0.48 °.

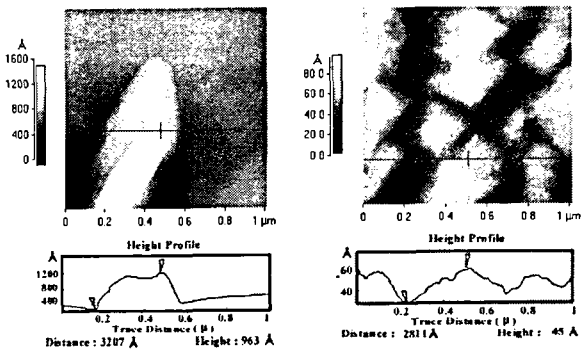

Fig. 3. AFM pictures of 400 nm-thick YBCO films (samples YBCO-A and YBCO-P2) on r-cut sapphire buffered with (a) an as-grown 45 nm-thick CeO_2 layer and (b) a post-annealed 45 nm-thick CeO_2 layer at 1000 °C.

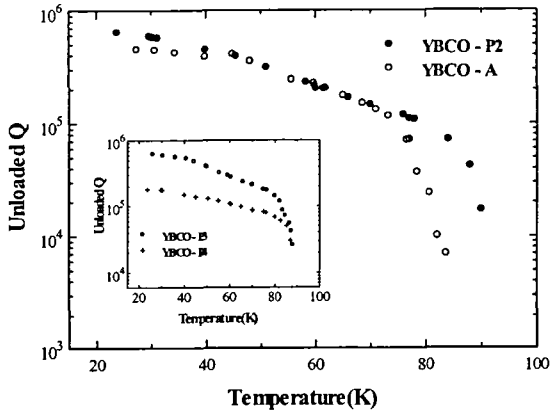

Fig. 4. The temperature dependence of the TE_{011} mode rutile-loaded cylindrical resonator with YBCO films (samples YBCO-A or YBCO-P2) as the endplates. Inset: The temperature dependence of the TE_{011} mode unloaded Q of the rutile-loaded resonator with samples YBCO-P3 or YBCO-P4 as the endplates.

the steps of reduced surface energy being the centers for the YBCO film growth and thereby allowing improved surface smoothness. However, further studies are needed to address the correct reasons for the improved surface smoothness.

We also measured the unloaded Q of an TE_{011} mode rutile-loaded cylindrical cavity resonator with the endplates replaced by samples YBCO-P2 ~ P4. Fig. 4 shows the unloaded Q (Q_0) vs temperature data for the rutile-loaded resonator with YBCO films used as the endplates. The resonant frequency is about 8.6 - 8.7 GHz at temperatures higher than 40 K. In the figure, Q_0 appears as high as 410000, 210000, and 72000 at 40 K, 60 K and 77 K, with sample YBCO-A used as the endplates. When sample YBCO-A was replaced by another sample YBCO-P2, Q_0 increased up to the values of 710000, 240000, and 110000 with the values significantly larger than the corresponding value of 410000, 210000, and 72000 at 40 K, 60 K and 77 K, observed with sample YBCO-A. The rutile-loaded cavity resonator with the other YBCO films on post-annealed CbS also appeared to have higher Q_0 when post-annealed CbS was used for YBCO film growth.

Summarizing, the surface smoothness of 400 nm-thick YBCO films on post-annealed CeO_2-buffered r-cut sapphire (CbS) appeared significantly improved when compared to those on as-grown CbS. YBCO films on post-annealed CbS at temperatures of 1000 – 1100 °C appeared to have the R-factor less than 1/10 of that of YBCO films on as-grown CbS, among which the YBCO film on post-annealed CbS at 1000 °C showed the most improved surface roughness with the R-factor of 4.5 nm. Besides, the 400 nm-thick YBCO films on post-annealed CbS also appeared to have much improved crystal structures, the FWHM of (005) peak rocking curve of 0.48 °, 0.46 ° and 0.47 ° for the YBCO films on post-annealed CbS at 1000 °C, 1050 °C and 1100 °C, respectively. The rutile-loaded cavity resonator with the 400 nm-thick YBCO films on post-annealed CbS at 1000 °C appeared to have high Q_0 with the values of 710000, 240000, and 110000 at 40 K, 60 K and 77 K, respectively, which were significantly larger than the corresponding value of 410000, 210000, and 72000 at 40 K, 60 K and 77 K, with the YBCO films on as-grown CbS substituted for the YBCO films on post-annealed CbS.

Acknowledgments

This work has been supported by Korean Ministry of Science and Technology and Ministry of Information and Communication under the university research program.

References

[1] R. Wördenweber, J. Einfeld, R. Kutzner, A. G. Zaitsev, M. A. Hein, T. Kaizer and G. Müller, IEEE Trans. Appl. Supercond. 9(2), 2486 (1999).

[2] E. K. Hollmann, O. G. Vendik, A. G. Zaitsev and B. T. Melekh, Supercond. Sci. Tech. 7, 609 (1994).

[3]. G.L. Skofronick, A. H. Carim, S. R. Foltyn, and R. E. Muenchausen, J. Mater. Res., vol.8(1993)2785

[4]. K. Frohlich, J. Souct, A. Rosova, D. Machajdik, I. E. Graboy, V. L. Svetchnikov, A. Figueras and F. Weiss, Supercond. Sci. Technol. 10(1997)657

[5] K. D. Develos, M. Kusunoki and S. Ohshima, Jpn. J. Appl. Phys. 37, 6161 (1998).

[6] R.-J. Lin, L.-J. Chen, L.-J. Lin, Y.-C. Yu, W. Wang, E.-K. Lin, Jpn. J. Appl. Phys. 35, 5805 (1996).

[7] M. Maul, B. Schulte, P. Haussler, J. Moses, M. Mathur, T. Venkatesan, J.C. Brasunas and B. Lakew : Appl. Phys lett, 67(1995), 1920.

[8] M. Maul, B. Schulte, P. Haussler, G. Frank, T. Steinborn, H. Fuess, H. Adrian: J. Appl. Phys. 74(4)1993, 2942

[9] M. W. Denhoyf, J. P. McCaffrey : J. Appl. Phys 79(7)1991. 3986.

[10] X. D. Wu, S. R. Foltyn, R. E. Muenchausen, D. W. Cooke, A. Pique, D. Kalokitis, V. Pendrick, E. Belohoubek: J. Supercon.5 (1992)353

[11] P. Berchant, R. D. Jacowitz, K. Tibbs, R. C. Taber, S. S. Laderman : Appl. Phys. Lett. 60(1992)763.

[12] I. E. Graboy, N. V. Markov, W. Maleev, A.R. Kaul, S. N. Polyakov, V. L. Svetchnikov, H. M. Zandbergen, K. H. Dahmen: Journal of Alloys and compounds 251(1997) 318.

[13] C. C. Chin, R. J. Lin, Y. C. Yu, C. W. Wang, E. K. Lin, W. C. Tsai, T. Y. Tseng : Physica C, 260(1996) 86.

[14] S. Y. Lee, H. J. Kwon, J. H. Lee, W. I. Yang and J. Hur, Supercond. Sci. Tech. 12, 833 (1999).

[15] I. E. Graboy, V. L. Svetchnikov, A. Figueras and F. Weiss, Supercond. Sci. Technol. 10, 657 (1997).

[16] J. H. Lee, W. I. Yang, H. J. Kwon, V. A. Komashko and Sang Young Lee, Supercond. Sci. Technol. 13, (2000), in press.

[17] B. H. Moechly, S. E. Russek, D. K. Lathrop, R. A. Buhrman, Jian Li, J. W. Mayer : Appl. Phys Lett 57, 1687 (1990).

[18] N. Klein, C. Zuccaro, U. Daehne, H. Schulz, and N. Tellman, J. Appl. Phys. 78(11), 6683-6686 (1995).